Computational and Electrochemical Study of Pyrantel as Alternative Green Corrosion Inhibitor of S275JR Mild Steel and 1100-H14 Aluminum Alloys in H2SO4 Acidic Environment

Benedict Ugi (ugibenedict@gmail.com)
University of Calabar https://orcid.org/0000-0003-0697-8280
Desmond Obi Nandi
University of Calabar

Research Article

Keywords: pyrantel, EIS, adsorption, Langmuir, S275JR mild steel, simulation

Posted Date: November 30th, 2022

DOI: https://doi.org/10.21203/rs.3.rs-2260824/v1

Computational and Electrochemical Study of Pyrantel as Alternative Green Corrosion Inhibitor of S275JR Mild Steel and 1100-H14 Aluminum Alloys in H_2SO_4 Acidic Environment

Abstract

The study on Recycling and application of Pyrantel as alternative corrosion inhibitor of S275JR mild steel and 1100-H14 aluminum alloys in 1 M H_2SO_4 acid environment was investigated adopting different experimental methods including weight loss, hydrogen evolution (gasometric), electrochemical impedance spectroscopic, potentiodynamic polarization and computational (quantum chemical calculations and molecular dynamic simulation) methods It was observed that pyrantel was a good inhibitor for both metals but with more inhibition on the 1100-H14 – type aluminum. Inhibition efficiency was recorded between 42.5 % and 95.2 % for aluminum at concentrations of 500 ppm and 1500 ppm respectively while 30.0 % and 72.5 % was recorded for S275JR mild steel at same concentrations as aluminum. This high inhibition efficient was attributed to the strong adsorption of the molecules on both metal surfaces. This result was in agreement with those of gasometric experiment. Electrochemical impedance showed higher and increasing values of charge transfer resistance and decreasing values for the double layer capacitance which indicated a better inhibition. From quantum calculations, the E_{HOMO} values was higher than that of the E_{LUMO} while the energy gap was calculated to be 1.9 with binding energy of 132.9. An indication that absorption was very strong and pyrantel is a good inhibitor. The data were in agreement with Langmuir adsorption isotherm as the correlation coefficient values were approximately unity indicating a physical adsorption and hence adsorption consists entirely of a monolayer at the surface.

Keywords: pyrantel, EIS, adsorption, Langmuir, S275JR mild steel, simulation

1. Introduction

Like death and taxes, corrosion is something we hope to avoid; but ultimately it is something we must learn to deal with. The fundamental cause or driving force for all corrosion is the lowering of a system's Gibbs energy [1-2]. The production of almost all metals (and engineering components made of metals) involves adding energy to the system. As a result of this uphill thermodynamic struggle, the metal has a strong driving force to return to its native, low energy oxide state. This return to the native oxide state is what we call corrosion and even though it is inevitable, substantial barriers (corrosion control methods) can be used to slow its progress toward the equilibrium state [1,3]. In the corrosion process, two reactions take place. In one, the anodic reaction, metal atoms are ionized and pass into solution leaving their electrons within the original metal surface [1-3]. In the second, the cathodic reaction, the free electrons within the metal are taken up by chemical species such as O_2 and H_2O in reduction reactions. Corrosion inhibitors have been found to be effective and flexible means of corrosion mitigation. Most of the organic/inorganic compounds containing elements of groups V B, VI B or functional groups of the type amine, carbonyl and alcoholic groups are more effective corrosion inhibitors [2,3-5]. The inhibitor is adsorbed on the entire metal surface and so prevents attack of the metal. Pyrantel is a carboxamidine that is 1,4,5,6-tetrahydropyrimidine that is substituted at position 1 by a methyl group and at position 2 by an (E)-2-(2-thienyl)vinyl group as shown in Fig. 1. It is used, particularly as the embonate [4,4'-methylenebis(3-hydroxy-2-naphthoate)] salt, as an anthelmintic that is effective against intestinal nematodes including threadworms, roundworms and hookworms. This

study is aimed at investigating Pyrantel application as alternative green corrosion inhibitor of S275JR mild steel and 1100-H14 aluminum alloys in 1 M H_2SO_4 acid environment.

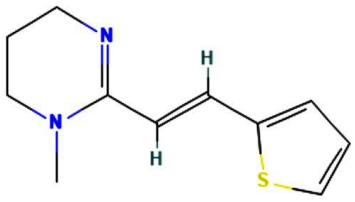

Fig. 1 Structure of Pyrantel (1,4,5,6-tetrahydropyrimidine)

2. Material and methods

2.1 Preparation of inhibitor stock Solution and Metal Dressing

5 g of the drug which was obtained in a powdered form was digested in a 1000 ml volumetric flask containing 1.0 M H_2SO_4 and allowed completely dissolve for 48 hours. It was later filtered and different inhibitor concentrations (500 ppm, 750 ppm, 1000 ppm, 1250 ppm and 1500 ppm) prepared. The piece of S275JR mild steel and 1100-H14 aluminum alloys used for this work were obtained from Ibom Metal and Aluminum Company, Akwa Ibom State, Nigeria with a composition of Fe (97.43%), C (0.2%), Si (0.05%), Mg (1.6%), S (0.05%), K (0.04%), and Cu (0.27%) for mild steel and Cu (0.05 – 0.20 %), Fe (0.95 %), Mn (0.05 %), Si (0.95 %), Zn (0.1 %), Residuals (0.15 %) and Al (98.8 %) for aluminum. The metals were resized into dimension 2.5 cm x 0.08 cm x 2.5 cm dimension for gravimetric analysis, 2.0 cm x 0.08 cm x 2.0 cm for gasometric analysis and 1 cm x 1 cm for electrochemical impedance analysis. All the resized metals were adequately polished with electronic UNIPOL- 820 metallographic polishing machine to a mirror surface with different grades of emery papers (300, 1000 and 1200 grades), washed in distilled water, degreased in ethanol, rinsed in Acrastrip 600 Auto reagent, air dried and stored in a moisture free desiccator.

2.2 Mass loss analysis

The polished coupons of dimension 2.5 cm x 0.08 cm x 2.5 cm were initially weighed and readings taken. They were then immersed in the individual free solutions of 1.0 M H_2SO_4 for 6 hours. The coupons were removed from the solutions, washed with distilled water, rinsed in ethanol, degreased with Acrastrip 600 Auto reagent and air dried then re-weighed. This procedure was repeated for the various concentrations on till the entire experimentation was completed for both metals. The surface coverage and % inhibition efficiency of inhibitor was determined from equation 1 and 2

$$Surface\ coverage\ (I) = \frac{(C_x - C_y)}{C_x} \ldots \ldots \quad \ldots \quad (1)$$

$$Inhibition\ efficiency(\%\ F) = \frac{(C_x - C_y)}{C_x} x100 \ldots \quad (2)$$

where I is the surface coverage of inhibitor, C_x and C_y are the corrosion rates of the free and inhibited solutions, $\%\ F$ is the percentage inhibition efficiency of the inhibitor.

2.3 Gasometric (Heat) analysis

Here, the prepared metal coupons of dimension 2.0 cm x 0.08 cm x 2.0 cm were at different occasion imersed into a solution of 1.0 M H_2SO_4 in a regulated water bath at temperatures of 303, 313, 323 and 333 K for 30 min each using a gasometric assembly. The metal coupons were retracted from the solution, washed with distilled water, rinsed in ethanol, degreased with Acrastrip 600 Auto reagent and air dried then weighed. This procedure was repeated for the various concentrations and different temperatures until the entire experimentation was completed. The surface coverage and % inhibition efficiency of inhibitor was determined from Equation 3 and 4.

$$Surface\ coverage\ (I) = \frac{(Cr_x - Cr_y)}{Cr_x} \ldots \quad \ldots \quad \ldots \quad (3)$$

$$Inhibition\ efficiency(\%\ \wp) = \left[1 - \frac{Cr_y}{Cr_x}\right] x100 \ldots \quad (4)$$

where I is the surface coverage of inhibitor, Cr_x and Cr_y are the corrosion rates of the free and inhibited solutions, $\%\ \wp$ is the percentage inhibition efficiency of the inhibitor.

2.4 Electrochemical method (EIS/PDP)

The EIS was conducted in a Gamry Reference 600 potentiostart/galvanostart inclusive of a Gamry framework EIS300 system. The fitting of the data was analyzed using the Echem Electro analyzer software. The reference electrode for the system was a saturated calomel (SCE) electrode and a 1cm^2 platinum foil was adopted as a counter electrode. The working electrode (mild steel and aluminum coupon) with dimension 1 cm x 1 cm was dipped in 1.0 M H_2SO_4 at different intervals. Electrochemical tests were conducted within a frequency of 10 Hz - 100,000 Hz within Potentiodynamic conditions, with an amplitude of 5 mV, involving alternating current signal at E_{corr}. The Potentiodynamic polarization measurement was carried out by altering the electrode potential from – 1.5 to + 1.5 V with respect to OCP at a scan rate of 0.01 mV/s. The data for corrosion density (I_{corr}) and corrosion potential (E_{corr}) were acquired automatically using Versa Studio software. All experiments were conducted every 60 min with the free and inhibited solutions. From the $b_{ct}^0$and I_{corr} obtained, the surface coverage and inhibition efficiencies was calculated using Equation 5 – 6 respectively.

$$I = \frac{b_{ct}^0 - b_{ct}^i}{b_{ct}^0} \ldots \ldots \quad \ldots \quad \ldots \quad \ldots \quad (5)$$

$$\%\ \wp = \frac{b_{ct}^0 - b_{ct}^i}{b_{ct}^0} x\ 100 \ldots \quad \ldots \quad \ldots \quad \ldots \quad (6)$$

$$\%\ \wp = 100\left[1 - \frac{I_{corr}^i}{I_{corr}^0}\right] \quad \ldots \quad \ldots \quad \ldots \quad (10)$$

where I is the surface coverage of the inhibitor, $b_{ct}^0$and b_{ct}^irepresent the charge transfer resistance and $I_{corr}^0$and I_{corr}^i is the corrosion density in the free and inhibited solutions of amiloride inhibitor respectively.

2.5 Computational method

This was carried out using a software Material Studio (version 8.0). The quantum chemical calculations were conducted using two (2) programs - the Vamp and Dmol[3]. And theoretical calculations were carried out at the Restricted Hartree-Fock level (RHF) using the Hamiltonian parametric method 3 (PM3). Information obtained include higher occupied molecular orbital

energy (E_{HOMO}), lower unoccupied molecular orbital energy (E_{LUMO}), Fukui positive and negative indices plots, HOMO and LUMO energy plots, energy gap (ΔE), chemical potential (μ), global hardness (η) and global softness (S), electrophilicity index (ω), according to **equation 7 – 11** respectively.

$$\text{Energy gap } (\Delta E) = E_{HOMO} - E_{LUMO} \quad \ldots \quad \ldots \quad \ldots \quad (7)$$

$$\text{Chemical potential } (\mu) = -\frac{(E_{HOMO}+E_{LUMO})}{2} \quad \ldots \quad \ldots \quad (8)$$

$$\text{Global hardness } (\eta) = \frac{(E_{HOMO}-E_{LUMO})}{2} \quad \ldots \quad \ldots \quad \ldots \quad (9)$$

$$\text{Global softness } (S) = \frac{1}{2\left[\frac{(E_{HOMO}-E_{LUMO})}{2}\right]} \quad \ldots \quad \ldots \quad \ldots \quad (10)$$

$$\text{Electrophilicity index } (\omega) = \frac{\mu^2}{2\left[\frac{(E_{HOMO}-E_{LUMO})}{2}\right]} \quad \ldots \quad \ldots \quad (11)$$

3. Result

3.1 Weight loss

From Tables 1-2, it was observed that the loosely bounded particles of the metal were affected by the acid attack especially where there was no inhibitor introduced. This could be due to the accumulation dissolved non - volatile metal particles in solution with time prompting an increased surface area on the metal [8, 10-13]. However, it was not the case when the inhibitor was added, it was noticed that the weight loss eventually began to decrease with time implying that the presence of the inhibitor gave rise to the reduction in the flow of electron from the anodic of the metal surface. This is again attributed to stronger phyto-atoms adsorption on the surface withholding the process of dissociation of loosely held particles [7, 11, 14].

Table 1. Weight loss data showing corrosion rate of 1100 – type aluminium, surface coverage and inhibition efficiency of pyrantel in 1m H_2SO_4 solutions

Conc.	Cor. Rate (mg/cm2/hr)	Sur. Cov.	Inh. Eff. (%)
Blank	0.0042	-	-
500 ppm	0.0025	0.405	40.5
750 ppm	0.0019	0.548	54.8
1000 ppm	0.0016	0.619	61.9
1250 ppm	0.0008	0.810	81.0
1500 ppm	0.0002	0.952	95.2

Table 2. Weight loss data showing corrosion rate of S275JR– type mild steel, surface coverage and inhibition efficiency of pyrantel in 1m H_2SO_4 solutions

Conc.	Cor. Rate (mg/cm2/hr)	Sur. Cov.	Inh. Eff. (%)
Blank	0.0040	-	
500 ppm	0.0028	0.300	30.0
750 ppm	0.0022	0.450	45.0

1000 ppm	0.0017	0.575	57.5
1250 ppm	0.0014	0.650	65.0
1500 ppm	0.0011	0.725	72.5

3.2 Gasometric Analysis

The plots from which the results of Tables 3 were obtained are shown in Figs. 2a-d for aluminum and corresponding plots and results for mild steel are shown in Fig. 3a -d and Table 4 respectively. The values in Table 3 and 4 showed that the inhibition was highly significant at lower temperatures for both metals. This lower inhibition efficiency as recorded following increased temperature is likely to be the effect of temperature agitation on the corrosion inhibition process, consequent upon the loosely bonded inhibitor molecules at the metal interface [6-9, 12]. The inhibition efficiency was found to be increasing following increased inhibitor concentration but decreasing with rise in temperature (Figs 2 and 3). This is an indication of stronger molecular adsorption [12-15]. Also this tendency can be attributed to a physical adsorption process and temperature dependent [13,15].

Table 3. Gasometric analysis data showing corrosion rate of 1100 – type aluminium, surface coverage and inhibition efficiency of pyrantel in 1M H_2SO_4 solutions

	303K			313K			323K			333K		
Inhibitor Conc.	CR (cm2/min)	θ	IE (%)	CR (cm2/min)	θ	IE (%)	CR (cm2/min)	θ	IE (%)	CR (cm2/min)	θ	IE (%)
Blank	0.811	-	-	1.001	-	-	1.119			2.099	-	-
500 ppm	0.517	0.363	36.3	0.821	0.180	18.0	0.932	0.167	16.7	1.963	0.065	6.5
750 ppm	0.322	0.603	60.3	0.622	0.379	37.9	0.744	0.335	33.5	1.574	0.250	25.0
1000 ppm	0.255	0.686	68.6	0.512	0.489	48.9	0.586	0.476	47.6	1.254	0.403	40.3
1250 ppm	0.178	0.781	78.1	0.330	0.671	67.1	0.562	0.497	49.7	1.164	0.445	44.5
1500 ppm	0.012	0.985	98.5	0.147	0.853	85.3	0.330	0.705	70.5	0.847	0.596	59.6

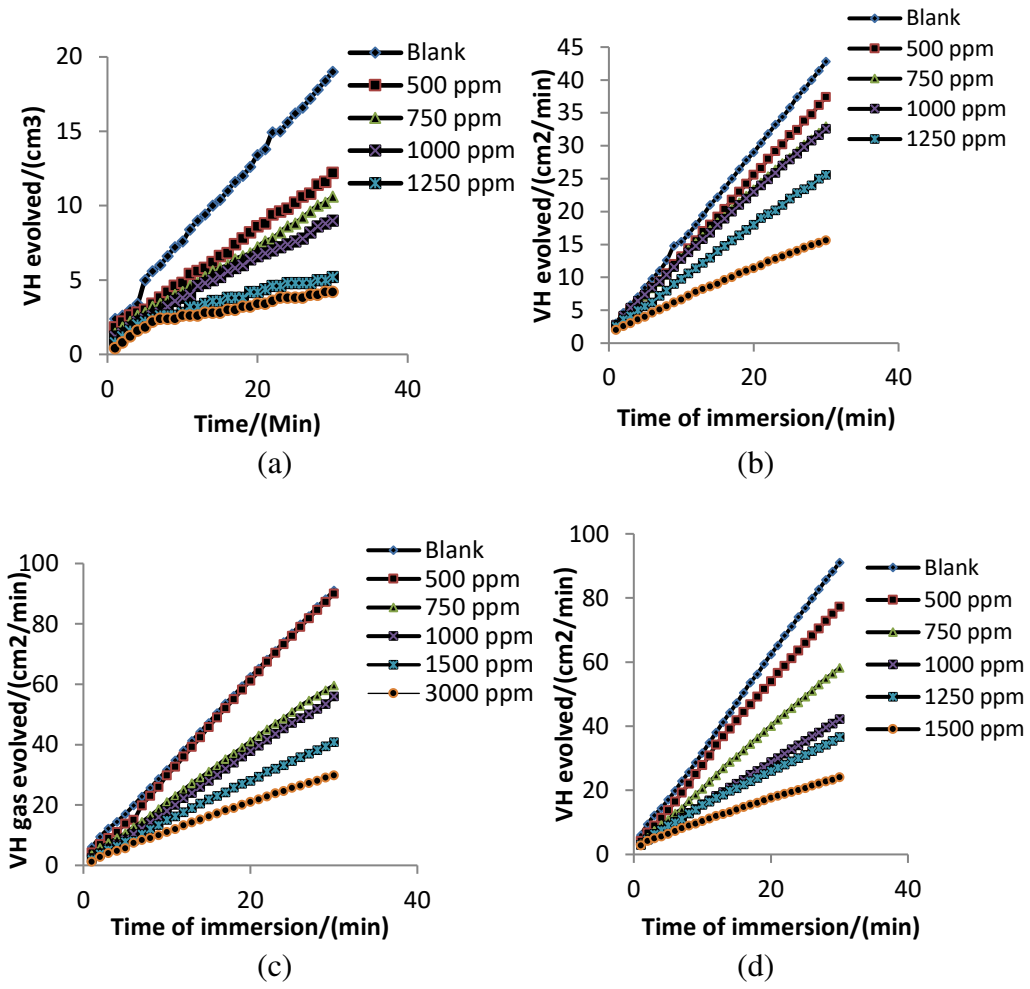

Fig. 2 Plot of volume of hydrogen gas evolved at (a) 303 K, (b) 313 K, (c) 323 K and (d) 333 K against immersion time for the corrosion of 1100 – type aluminum with and without pyrantel inhibitor in 1 M H_2SO_4 solutions

Table 4. Gasometric analysis data showing corrosion rate of S275JR – type mild steel, surface coverage and inhibition efficiency of pyrantel in 1M H_2SO_4 solutions

	303K			313K			323K			333K		
Inhibitor Conc.	CR (cm2/min)	θ	IE (%)	CR (cm2/min)	θ	IE (%)	CR (cm2/min)	θ	IE (%)	CR (cm2/min)	θ	IE (%)
Blank	0.811	-	-	1.001	-	-	1.119			2.099	-	-
500 ppm	0.453	0.441	44.1	0.517	0.484	48.4	0.835	0.254	25.4	1.663	0.208	20.8
750 ppm	0.389	0.520	52.0	0.466	0.534	53.4	0.786	0.298	29.8	1.532	0.270	27.0
1000 ppm	0.213	0.737	73.7	0.382	0.618	61.8	0.719	0.357	35.7	1.383	0.341	34.1
1250 ppm	0.174	0.785	78.5	0.265	0.735	73.5	0.527	0.529	52.9	1.107	0.473	47.3

1500 ppm	0.096	0.882	88.2	0.174	0.826	82.6	0.386	0.655	65.5	0.900	0.571	57.1

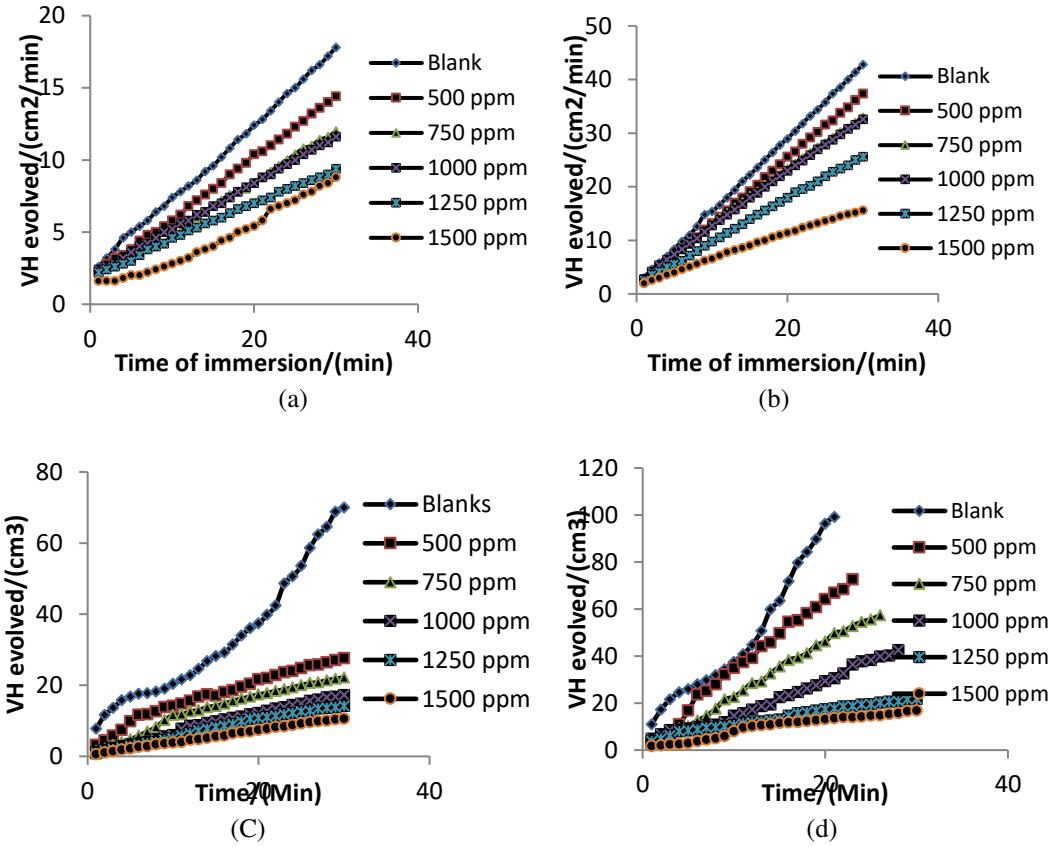

Fig. 3 Plot of volume of hydrogen gas evolved at (a) 303 K, (b) 313 K, (c) 323 K and (d) 333 K against immersion time for the corrosion of S275JR – mild steel with and without pyrantel inhibitor in 1 M H_2SO_4 solutions

3.3 Electrochemical impedance spectroscopy

Data for the electrical interference of the system with the inhibitor are presented in Table 5 and 6 and the corresponding Nyquist plots are shown in Figs. 4 and 5a-b. It was observed that the inhibitor presented a single capacity loop for both S275JR - Mild steel and 1100 - Aluminum which is directed towards a single charge transfer [6, 15-17]. The sizes of these loops were observed to increases with the rise up to 2500 ppm which is in line with the increased charge transfer values indicating an adsorption of the inhibitor on both surfaces and a reduction of the exposed area (active sites) of the metal [10,15,16]. The data for the double-layer capacitance of the semicircle and inhibition efficiency were determined following Equation 12 - 13 and are presented in Table 5 and 6.

$$C_{dl} = \frac{1}{\omega Z''} \ldots \quad \ldots \quad \ldots \quad \ldots \quad (12)$$

where Z" is imaginary component of impedance at any frequency inside the semicircle and ω is the angular frequency [9,11].

$$\% \wp = \frac{b_{ct}^{0} - b_{ct}^{i}}{b_{ct}^{0}} x\ 100 \ldots \quad \ldots \quad \ldots\ldots \quad (13)$$

where b_{ct}^{0} and b_{ct}^{i} correspond to the charge ransfer values in the free and inhibited solutions of expired pyrantel inhibitor respectively.

Values from Table 5 and 6 shows increased charge transfer resistance as both metals were measured through increased concentration. Considering the increase values of the charge transfer resistance with inhibitor concentrations, it implies that a greater difficulty and energy lost was encountered during the inhibition process in the presence of the pyrantel inhibitor as the electrochemical process was effected, hence strong surface adsorption came to play as well as inhibition of corrosion active sites in metal [18-20].

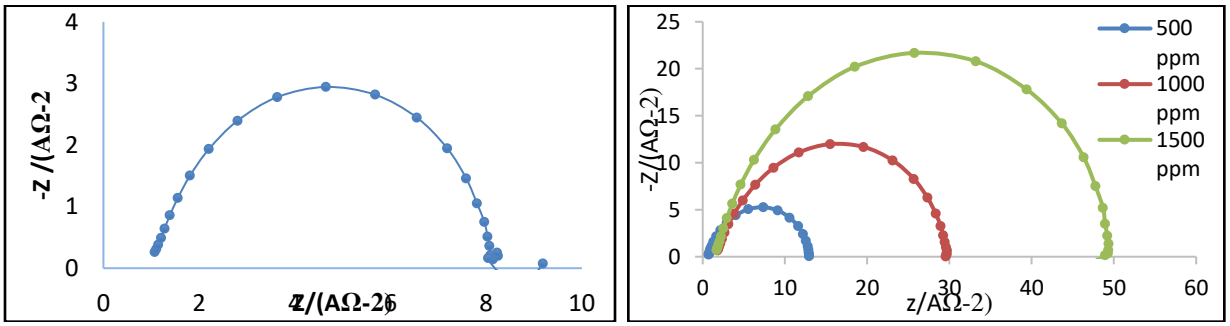

(a) (b)

Fig. 4 Nyquist plots for the corrosion inhibition of S275JR – type mild steel (a) without and (b) with pyrantel inhibitor in 1 M H_2SO_4 solutions

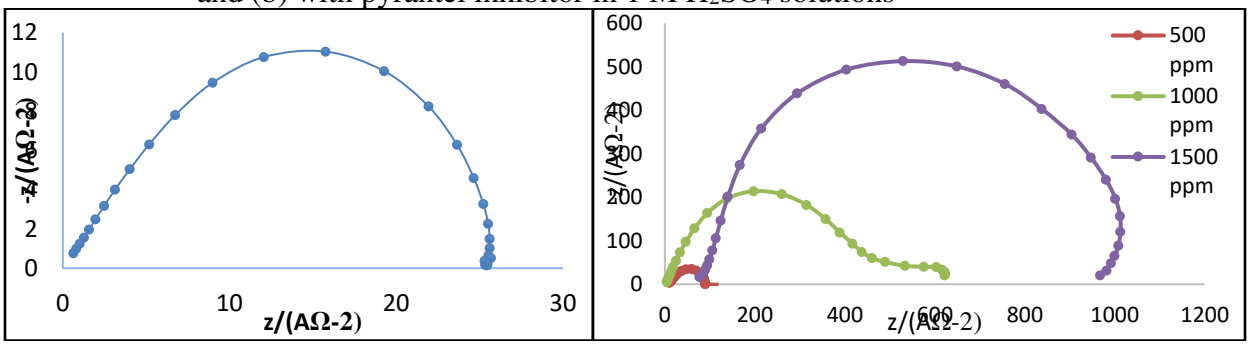

(a) (b)

Fig. 5 Nyquist plots for the corrosion inhibition of 1100 – type aluminum (a) without and (b) with pyrantel inhibitor in 1 M H_2SO_4 solutions

Table 5. Nyquist plots values showing charge transfer resistance, double layer capacitance and inhibition efficiency for the corrosion inhibition of S275JR – type mild steel using pyrantel inhibitor in 1 M H_2SO_4 solutions

Conc. (ppm)	R_{ct} ($A^{-2}\Omega$)	C_{dl}	IE (%)
Blank	7.0	2.411 x 10^{-5}	
500	13.7	1.749 x 10^{-5}	48.9

1000	30.1	1.545 x 10^{-5}	76.7
1500	48.5	1.516 x 10^{-5}	85.9

Table 6. Nyquist plots values showing charge transfer resistance, double layer capacitance and inhibition efficiency for the corrosion inhibition of 1100 – type aluminum using pyrantel inhibitor in 1 M H_2SO_4 solutions

Conc. (ppm)	R_{ct} ($A^{-2}\Omega$)	C_{dl}	IE (%)
Blank	26.4	6.658 x 10^{-6}	-
500	97.6	4.586 x 10^{-6}	72.9
1000	658	2.506 x 10^{-6}	95.9
1500	889	2.267 x 10^{-6}	97.0

In order to analyze the electrochemical system stability during the corrosion inhibition process with and without the inhibitor, the Phase margins of the Bode plots were derived from the electrochemical experiment as shown in Fig. 6a-b). Bode plots are useful in analyzing magnitude and phase changes introduce by a liner time invariant system through the controlled loop response [5-6, 19-22]. Gains and phase margins represent the distance from the point at which instability could occur. The greater the distance or margin, the better, because higher gains or phase margins means greater stability [18-19].To determine the phase magine, the equation 14 was adopted.

$$Pm = \emptyset - (-180^0) \quad \ldots \qquad \ldots \qquad (14)$$

Where $\emptyset$ is the phase lag (a number less than zero).

From the plots (Fig. 6a-b), it was observed that all the phase lag data fitted to the equation 14 gave rise to a positive phase margin and higher values (i.e. for mild steel, Blank – 138^0, 500 ppm - 130^0, 1000 ppm - 120^0 and 1500 ppm - 130^0 and for aluminum, Blank – 120^0, 500 ppm - 139^0, 1000 ppm - 113^0 and 1500 ppm - 125^0). This implies that the system was perfectly stabilized by the inhibitor throughout the electrochemical process which makes the pyrantel inhibitor a good one for the corrosion inhibition of the metals [21-23].

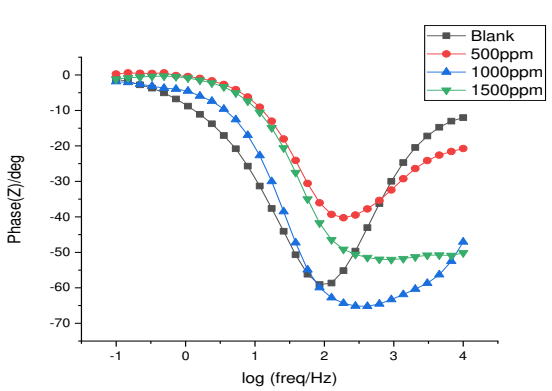

(a)

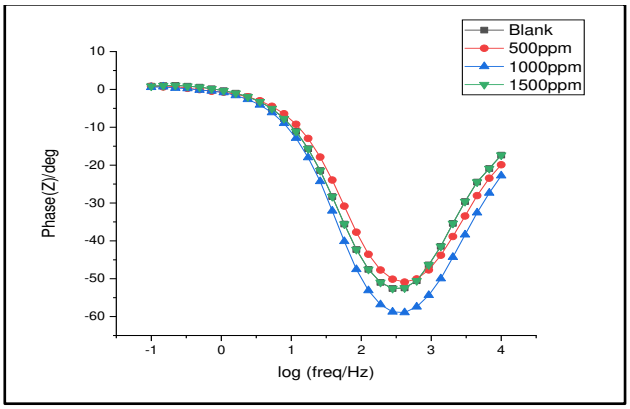

(b)

Fig. 6 Bode plots for the corrosion inhibition of (a) 1100 – type aluminum (b) S275JR – type mild steel using pyrantel inhibitor in 1 M H_2SO_4 solutions

3.4 Potentiodynamic polarization

Table 7 and 8 shows values of potentiodynamic polarization result deduced from Figure 7a - b. It was confirmed that the corrosion potential values were shifted gradually to a more positive direction at every addition of the inhibitor, and also shows changes in both the cathodic and anodic polarization branches. This as an indication that the added inhibitor molecules acted majorly as an anodic type inhibitor [15, 19-21]. This can also be confirmed from the anodic and cathodic Tafel slope values in Table 7and 8. The corrosion current density values were found to be decreasing while those of the corresponding inhibition efficiency obtained from corrosion polarization were increasing for both metals in the presence of the inhibitor. Which it implies that the loss of electrons at the anode was minimal, there was no trigger of oxidation reaction that would have caused the anode to deteriorate (corrode). Hence the cathode remains unaffected [23-25].

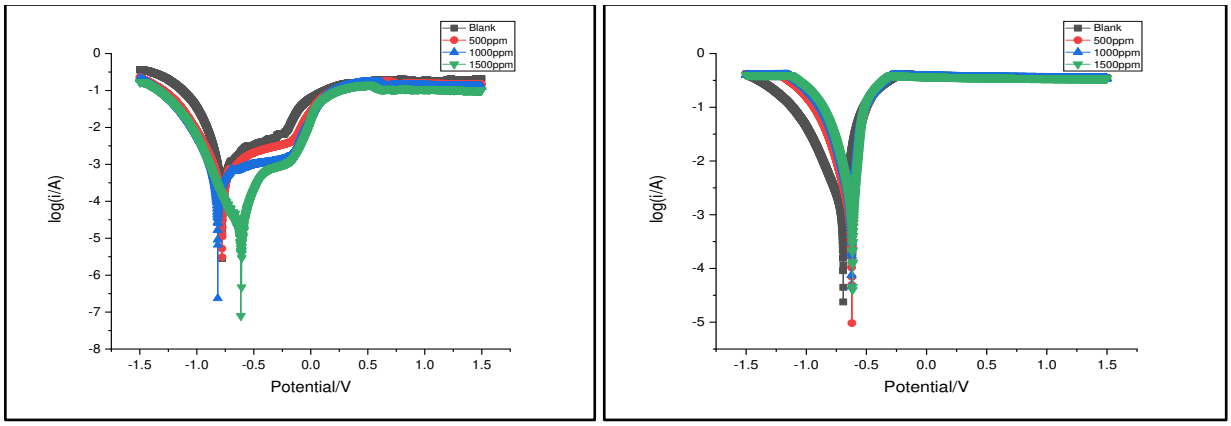

Fig. 7 Tafel plots for the corrosion inhibition of (a) S275JR – type mild steel and (b) 1100 – type aluminum using pyrantel inhibitor in 1 M H_2SO_4 solutions

Table 7. Tafel plots values for the corrosion inhibition of 1100 – type aluminum using pyrantel inhibitor in 1 M H_2SO_4 solutions

Conc. (ppm)	I_{corr} (μAcm^{-2})	Slp_c (mV/dec)	Slp_a (mV/dec)	LP (Ω)	IE_{LP} (%)	IE_{Icorr} (%)	E_{corr} (mV)
Blank	9.905	9.706	8.211	1067	-	-	-9.368
500	4.231	7.969 [1.737]	4.179 [4.042]	116	89.1	57.3	-7.256
1000	3.366	7.765 [1.941]	2.661 [5.563]	106	90.1	66.0	-6.758
1500	3.138	4.763 [4.943]	1.412 [6.809]	53	95.0	68.3	-6.405

Table 8. Tafel plots values for the corrosion inhibition of S275JR – type mild steel

using pyrantel inhibitor in 1 M H_2SO_4 solutions

Conc. (ppm)	I_{corr} (μAcm^{-2})	Slp_c (mV/dec)	Slp_a (mV/dec)	LP (Ω)	IE_{LP} (%)	IE_{Icorr} (%)	E_{corr} (mV)
Blank	3.296	9.238	10.669	27	-	-	-5.596
500	1.848	8.738 [0.500]	10.599 [0.110]	15	44.4	43.9	-5.071
1000	1.778	8.619 [0.619]	9.865 [0.804]	12	55.6	46.1	-4.964
1500	1.377	5.618 [3.620]	8.812 [1.857]	8	70.4	58.2	-4.734

3.5 Quantum chemical calculations

The E_{HOMO} and E_{LUMO} were used to calculate the global quantum chemical indices. Fig. 8a -c shows the optimized structure and the Frontier molecular orbitals (FMO) distribution density of the energy of highest occupied molecular orbital (E_{HOMO}) and the energy of lowest unoccupied molecular orbital (E_{LUMO}) for pyrantel. It is evident from the figures that the electron density distribution at the highest occupied molecular orbital (HOMO) is localized strongly on the heteroatom (Nitrogen), carbon – carbon double bonds on the aromatic benzene ring and in methyl group (CH_3) present in pytantel [17-19]. However, the electron density distribution for the lowest unoccupied molecular orbital (LUMO) was distributed on the individual carbon atoms on the aromatic ring and on the Sulphur stereogenic centers. Therefore the inhibitory power of pyrantel can be explained mostly by the presence of π electrons and nitrogen heteroatoms favoring the sharing of electrons between inhibitor and the metal surface [10-12, 23-26].

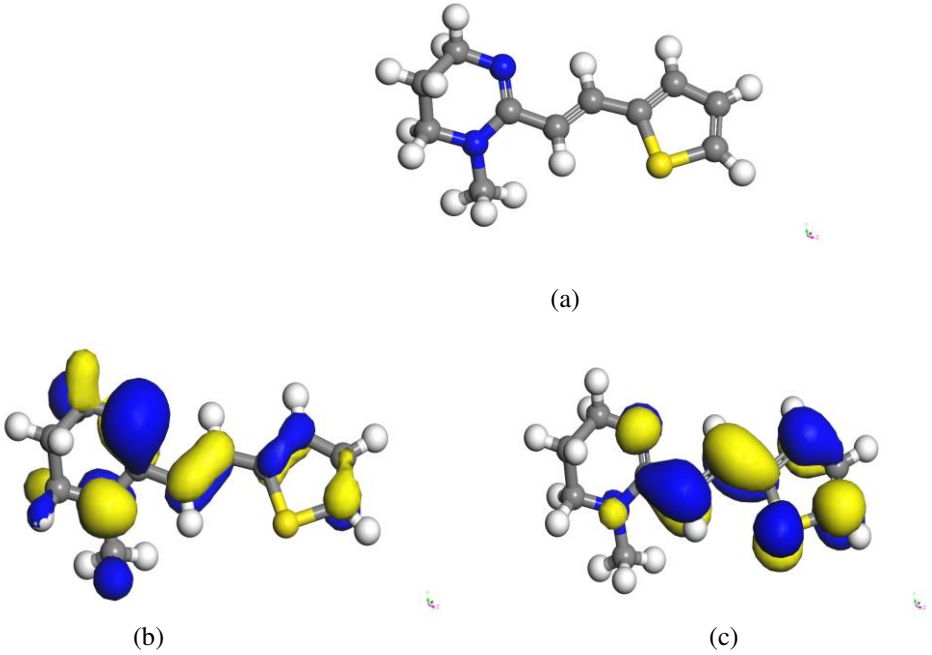

(a)

(b) (c)

Fig. 8 (a) Optimized structure, (b) Highest occupied molecular orbital and (c) Lowest unoccupied molecular orbital of pyrantel molecule

Table 9 shows the quantum chemical parameters for pyrantel as inhibitor of corrosion of S275JR mild steel and 1100 aluminum. Absolute electronegativity (χ), global hardness (η), global softness (σ), electrophilicity index (ω), nucleophilicity index (δ)

$$\chi = \frac{I.P.+E.A.}{2} \quad \ldots \quad \ldots \quad \ldots \quad (15)$$

$$\eta = \frac{I.P.- E.A.}{2} \ldots \quad \ldots \quad \ldots \quad (16)$$

$$\sigma = \frac{1}{\eta} \quad \ldots \quad \ldots \quad \ldots \quad \ldots \quad (17)$$

$$\omega = \frac{\chi 2}{2\eta} \quad \ldots \quad \ldots \quad \ldots \quad (18)$$

$$\delta = \frac{1}{\omega} \quad \ldots \quad \ldots \quad \ldots \quad \ldots \quad (19)$$

where φ_m is the work function for the metal surface (work function for Fe (110) is 4.82eV while that of Al (111) is 4.02eV), χ_i represents absolute electronegativity of the inhibitor, η_m and η_i represents global hardness for the metal and inhibitor respectively. **I**t was observed that the value of E_{HOMO} was higher compared to that of E_{LUMO} which signifies that the inhibitor has higher tendency to donate electrons to the appropriate acceptor molecule of low empty molecular orbital energy (metal surface). This can be verified from the ΔE value as the inhibitor has a lower energy gap (2.46 eV) suggesting an easier polarization of the molecule and a lower energy requirement for the removal of an electron from the highest occupied orbital which entails a better inhibitor [16, 21, 26]. From Table 9, the value of the hardness was higher compared to that of softness. This implies that theirs is a shorter energy gap between the inhibitor/metal interface and a possible lower dissociation energy giving rise to stronger adsorption and a better inhibition [22, 26-28]. Also, the global electrophilicity index (ω) has a value of 5.045, implying a higher inhibition efficiency [28].

Table 9. Quantum chemical calculations values for pyrantel molecule

Parameters	Data (eV)
E_{HOMO}	-4.075
E_{LUMO}	-2.154
ΔE (energy gap)	1.921
χ	3.114
η	0.961

σ	1.848
ω	5.045
δ	0.198
ΔN	2.969
ΔE_{b-d}	0.240
Binding energy	-132.9

In order to examine the influence of the heteroatoms on the inhibition efficiency, the local reactivity was analyzed by evaluating the Fukui indices (Fig. 9). In the electrochemical series, nitrogen is more electronegative than sulphur hence, the results revealed that N (4) and N (6) are most prone to attack by an electrophilic site hence likely to accept electrons from the metal, while S (14)), C (8), C (9), C (11) and C (13) is most prone to attack by a nucleophile site hence likely to donate electrons to the metal [14-16, 27]. Fig. 10a- d also confirms that the surface is highly concentrated at N (4), N (6) and S (14) atoms which acts as the most reactive site of pyrantel molecule for donor-acceptor.

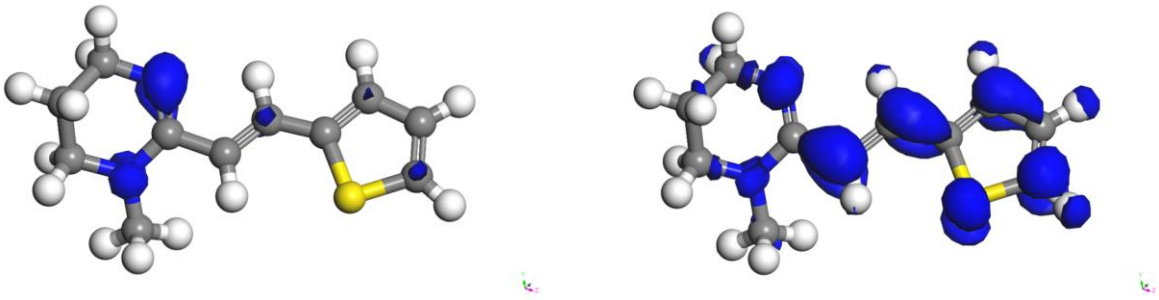

(a) (b)

Fig. 9a - b Fukui function (a) Electrophilic (f^-) and (b) Nucleophilic (f^+) reactive sites of pyrantel molecule

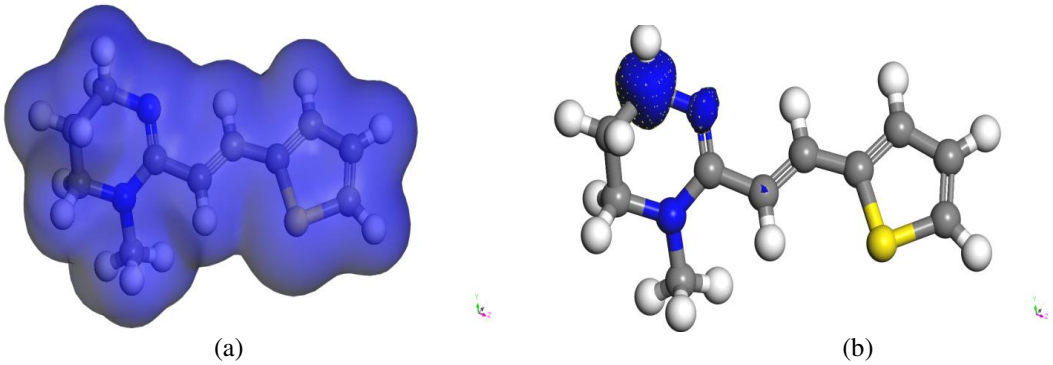

(a) (b)

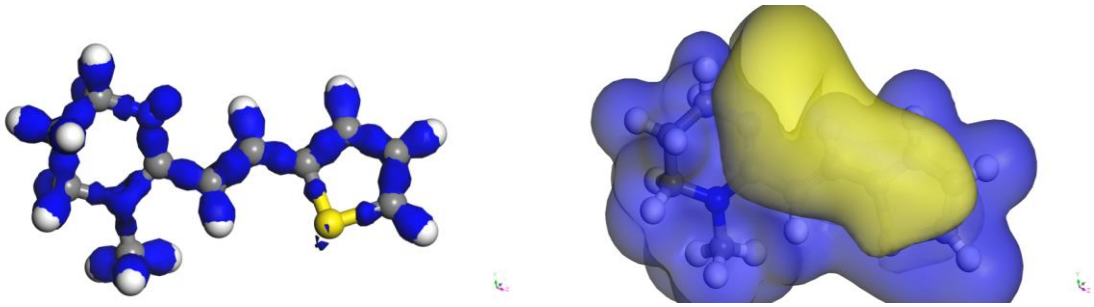

(c) (d)

Fig. 10 (a) Total electron density (b) Spin density (c) Deformation density and (d) Molecular electrostatic potential of pyrantel molecule

3.6 Molecular simulation dynamics

The lower energy of inhibitor adsorption configurations on the Fe (110) and Al surfaces are shown in Fig. 11a-c. As presented in Fig. 11a - c, π-electrons of the benzene rings, Nitrogen and Carbon atoms are the major adsorption centres of the examined inhibitors on the surface of Fe (110) and Al (111). Inhibitor molecules are adsorbed in a nearly flat orientation on the iron surface compared to aluminium surface to maximize coating and surface contact, providing a strong interaction for the adsorbate/substrate system for the iron [11-12, 21, 28]. The inhibitor molecules adsorbed nearly plane on the aluminum (111) surface to maximize surface coverage and contact, ensuring a strong interaction between adsorbate and substrate. This finding is in good agreement with the experimental results.

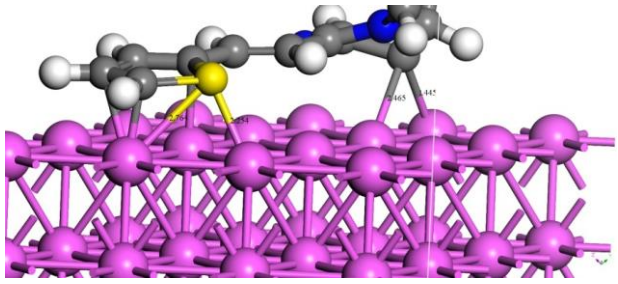

(a)

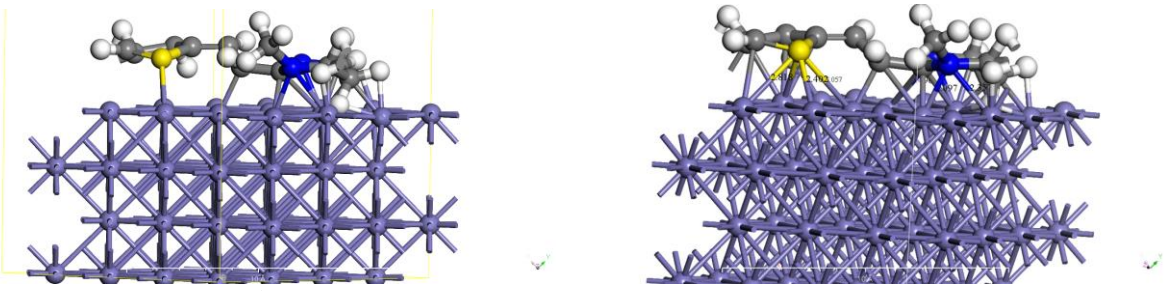

(b) (c)

Fig. 11 (a) Bond length (b) adsorption of pyrantel (Inhibitor) on Iron (Fe 110)

surface (Across View) (c) Fe/pyrantel Adsorption process showing bond length of selected heteroatoms of pyrantel molecule

3.7 Thermodynamic result

Values of standard free energy of adsorption, ΔG^{*}_{ads} and equilibrium constant k were obtained from the reciprocal of the intercept of Fig. 12a - b according to equation 20 [9].

$$k = \frac{1}{55.5}\exp\frac{-\Delta G_{ads}}{RT} \quad \ldots \quad \ldots \quad \ldots \quad (20)$$

The calculated ΔG^{*}_{ads} values are listed in Table 10. The negative values of adsorption free energy for both metals indicate that the inhibition process is spontaneous in the forward direction, the inhibitor is very stables on the metal surface and physically [13-16, 22]. The observed ΔG^{*}_{ads} values (Table 10) supported the mechanism of following the fact that ΔG^{*}_{ads} values greater than -40KJmol^{-1} denotes physisorptions. In examining the effect of temperature on the corrosion inhibition process, the apparent activation energy (Ea) was calculated from the Arrhenius equation 21 and plots in Fig. 12 a - b.

$$log\frac{Ra}{Rb} = \frac{Ea}{2.303R}\left(\frac{1}{T1} - \frac{1}{T2}\right) \quad \ldots \quad \ldots \quad (21)$$

where Ra and Rb are the corrosion rates at temperature T1 and T2 respectively, and R the molar gas constant. It is seen from Table 10 that Ea values were higher in the presence of pyrantel in both metals acid solutions compared to those in the absence of the inhibitor leading to a decrease in their corrosion rates.

Table 10. Thermodynamic data reporting collision coefficient, energy of activation, enthalpy and entropy of adsorption for the corrosion of MS and Al in 1 M H_2SO_4

	Inh. Conc.	A (ML^{-1}s^{-1})	Ea (kJmol^{-1})	ΔH (kJmol^{-1})	ΔS (kJmol^{-1})
MS	Blank	2.0	19.1	8.31	-857.1
	500 ppm	1.9	19.8	15.8	-160.5
	750 ppm	2.5	34.9	19.1	-193.7
	1000 ppm	2.1	21.6	24.9	-251.9
	1250 ppm	2.6	32.4	27.4	-276.9
	1500 ppm	2.6	38.2	49.8	-501.4
Al	500 ppm	2.3	29.0	12.5	-127.2
	750 ppm	2.2	27.4	13.3	-138.6
	1000 ppm	2.8	47.3	31.6	-318.5
	1250 ppm	3.1	64.0	44.9	-451.5
	1500 ppm	3.5	93.1	75.7	-759.1

The transition state equation as represented in Equation 22 was used in obtaining the enthalpy and entropy of adsorption through plots as shown in Figs. 13a - b

$$\log \frac{CR}{T} = log\ \frac{R}{Nh} + \frac{\Delta S}{2.303R} - \frac{\Delta H}{2.303RT} \quad \ldots \quad \ldots \quad (22)$$

The positive values of ΔH^o indicated that the dissolution of the metal was an endothermic reaction [10-11, 28-30]. The change in entropy ($\Delta S°$) was found to be greater than zero. This indicates that the reaction is irreversible hence inhibition is favoured and the pyrantel a better inhibitor for the metals in the examined acid solution and the complete desorption of the inhibitor is not possible in both acid media [9, 17-19]. The shift towards negative values of entropy ($\Delta S°$) as recorded in Table 11 for both metals implied that the activated complex in the rate determining step represents association rather than dissociation [19-21].

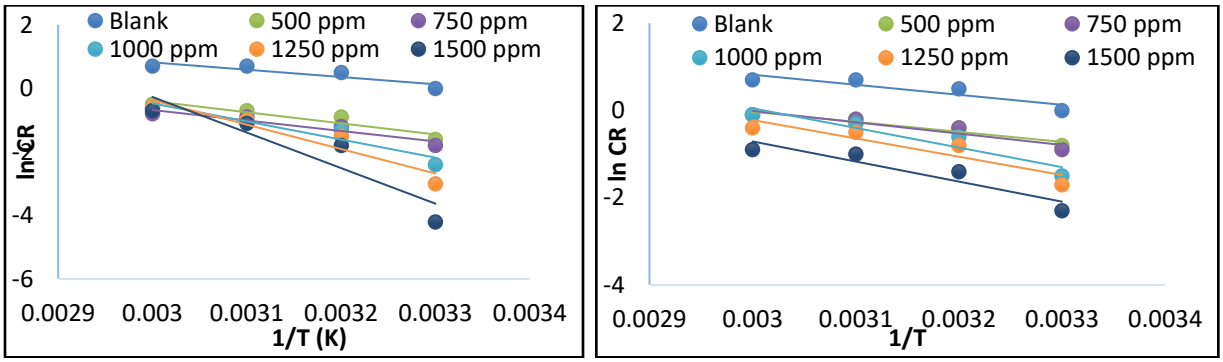

(b)

Fig. 12 Arrhenius plots for the corrosion of (a) 1100 – type aluminum and (b) S275JR – type mild steel in the absence and presence of pyrantel inhibitor in 1 M H_2SO_4

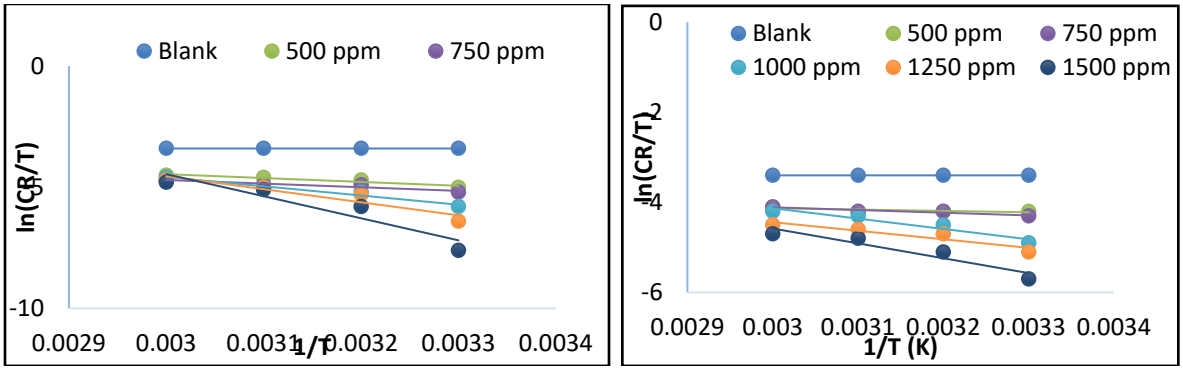

(b)

Fig. 13 Transition state plots for the corrosion of (a) 1100 – type aluminum and (b) S275JR – type mild steel in the absence and presence of pyrantel inhibitor in 1 M H_2SO_4

3.8 Adsorption result

To investigate the level of adsorption and mechanism, Langmuir, adsorption isotherm was introduced and determined from equation 23

$$\frac{C}{\theta} = \frac{1}{k} + C \quad \ldots \quad \ldots \quad (23)$$

Assessment of Table 12 and Fig. 14 shows that the equilibrium constant values (were increasing with temperature which explains a physical adsorption confirming the temperature dependent results that describes the inhibitor as perfect at lower temperatures [21-22, 31-33]. This result also indicates that more formation of bonds between the inhibitor and the metal was possible hence leading to inhibition [12, 19, 34] The values of the correlation coefficient showed that Langmuir assumption was obeyed, hence adsorption consist entirely of a monolayer at the surface and there is no interaction inhibitor molecules on different sites of the metals and each metal active site can hole only one adsorbed inhibitor molecule. Also it implies that the heat of adsorption regarding the inhibitor – metal interaction does not depend on the number of sites but is equal for all sites which makes the inhibitor a better one and confirmed the earlier results from weight loss analysis [35-39]

Table 12 Langmuir adsorption isotherm data for the corrosion of MS and Al in 1 M H_2SO_4

	Aluminum				Mild steel			
Temp.	k	R	slope	ΔG	k	R	slope	ΔG
303 K	3.2 x 10^{-3}	0.9995	0.8529	-4.78	2.1 x 10^{-3}	0.9073	0.9074	-5.95
313 K	3.6 x 10^{-3}	0.9992	1.0619	-4.33	2.8 x 10^{-3}	0.9543	1.1254	-4.69
323 K	4.1 x 10^{-3}	0.9798	1.0334	-3.72	4.6 x 10^{-3}	0.9773	1.1906	-3.55
333 K	5.4 x 10^{-3}	0.9779	1.0825	-3.14	4.7 x 10^{-3}	0.9672	1.0750	-3.61

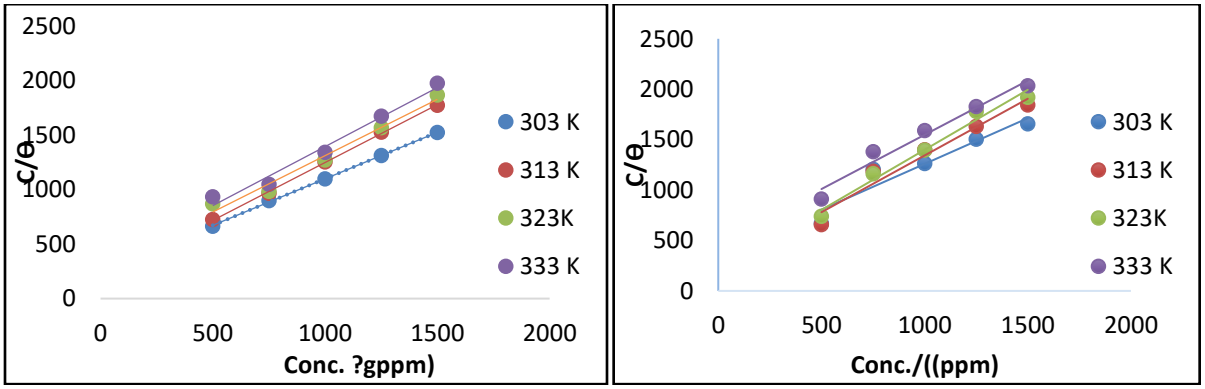

(b)

Fig. 14 Langmuir isotherm plots for (a) 1100 – type aluminum and (b) S275JR – type mild steel

Conclusion

1. Arising from all the experimental techniques under study, it is confirmed that

pyrantel was a reliable alternative inhibitor for the inhibition of both mild steel and aluminum corrosion in sulphuric acid environment.

2. Inhibition of corrosion on both metals was observed to be through strong adsorption of pyrantel molecules on the surface of the metals.

3. Pyrantel as alternative inhibitor demonstrated a stabled nature (lesser degree of disorderliness), spontaneous and physical adsorption process which made it a better inhibitor.

4. Electrochemical data was in good agreement with those of the chemical and theoretical as charge transfer resistance and inhibition efficiency were increasing while the double layer capacitance was decreasing with concentration respectively. Features that are attributed to a good inhibitor.

5. Theoretical data shows that the inhibitor was good as the energy gap for pyramtel was as low as 1.921 ev and inhibition depend largely on the hetero-atoms of the major constituent of pyrantel.

Statement and Declaration

Competing interest: The authors declare that there is no conflict of interest in the research work.

Funding: the authors received no funding for this research. It was a self-sponsored research.

References

[1]. Abdallah M, Gad EAM, Sobhi M (2019) Performance of tramadol drug as a safe inhibitor for aluminum corrosion in 1.0 M HCl solution and understanding mechanism of inhibition using DFT. Egyptian J Petrol 28:173-181 http://doi.org./10.1016/j.ejpe.2019.02.003

[2]. Agwamba EC, Udoikono AD, Hitler L (2022) Synthesis, characterization, DFT studies, and molecular modeling of azo dye derivatives as potential candidate for trypanosomiasis treatment. Chem Phys Impact 4:100076 http://doi.org./10.1016/chphi.2022.100076

[3]. Ameh PO, Eddy NO (2018) Experimental and computational chemistry studies on the inhibition efficiency of phthalic acid (PHA) for the corrosion of aluminum in hydrochloric and tetraoxosulphate (VI) acids. Protec Met Phy Chem Surf 2:1-13. http://doi.org./10.1134/S2070205118060035

[4]. Ammouchi N, Allal H, Belhocine Y (2020) DFT computations and molecular dynamics investigations on conformers of some pyrazinamide derivatives as corrosion inhibitors for aluminum. J Mol Liq 300:112309. http://doi.org./10.1016/j.molliq.2019.112309

[5]. Bashir S, Sharma V, Kumar S (2020) Inhibition performances of Nicotinamide against aluminum corrosion in an acidic medium. Port Electrochim Acta 38:107-123. http://doi.org./10.4152/pea.202002107

[6]. Ugi BU (2021) Corrosion Inhibition of Cu-Zn-Fe Alloy in Hydrochloric Acid Medium by Crude Ethanol Extracts from Roots-Leaves Synergy of Solanum melongena. Earthline J. Chem. Sci 5(1): 105 - 118

[7]. Bai Y, Sui H, Liu X (2019) Effects of the N, O, and S heteroatoms on the adsorption and desorption of asphaltenes on silica surface: a molecular dynamics simulation. Fuel 240: 252–261. http://doi.org./ 10.1061/j.fuel.2018.11.135

[8]. Bharatiya U, Gal P, Agrawal A (2019) Effect of corrosion on crude oil and natural gas pipeline with emphasis on prevention by ecofriendly corrosion inhibitors: a comprehensive review. J Bio – Tribo Corr 5:35 http://doi.org./10.1007/s40735-019-0225-9

[9]. Bhuvaneswari M, Santhakumari R, Usha C (2021) Synthesis, growth, structural, Spectroscopic, optical, Thermal, DFT, HOMO–LUMO, MEP, NBO analysis, and Thermodynamic properties of vanillin isonicotinic hydrazide single crystal. J Mol Struct 4: 130856. http://doi.org./10.1016/j.molstruc.2021.130856

[10]. Boumhara K, Harhar H, Tabyaoui M (2019) Corrosion inhibition of mild steel in 0.5 M H_2SO_4 solution by Artemisia herba- alba Oil. J Bio – Tribo Corr 5:1-8 http://doi.org./10.1007/s40735-018-0202-8

[11]. Ugi BU, Obeten M (2019) Inhibition of Limestone ($CaCO_3$) Concentrated Rich Water Effects On Zinc Sheets Using Crude Alkaloids and Non Alkaloid s Extracts of *Nepeta cataria* (Catnip) Plant. *Int. J. Innov. Sci. Engr. Techno 6(3): 74 - 81*

[12]. Dagdag O, El Harfi A, Cherkaoui O (2019) Rheological, electrochemical, surface, DFT and molecular dynamics simulation studies on the anticorrosive properties of new epoxy monomer compound for steel in 1 M HCl solution. *RSC Advance* 9:4454–4462. http://doi.org./10.1039/c8ra09446b

[13]. Diki NYS, Coulibaly NH, Kambire O (2021) Experimental and theoretical investigations on copper corrosion inhibition by cefixime drug in 1 M HNO3 solution, J Mater Sci Chem Engr 9: http://doi.org./10.4236/msce.2021.95002

[14]. Dimakis N, Salas I, Gonzalez L (2019) Li and Na adsorption on graphene and graphene oxide examined by density functional theory, quantum theory of atoms in molecules, and electron localization function. Molecules 24:754. http://doi.org./10.3390/molecules24040754

[15]. Ebenso EE, Verma C, Olasunkanmi LO (2021) Molecular modelling of compounds used for corrosion inhibition studies: a review. Phys Chem Chem Phys 23:19987 – 20027 http://doi.org./10.1039/D1CP00244A

[16]. El-Monem MA, Shaban MM, Khalil MMH, (2020) Synthesis, Characterization and computational chemical study of Aliphatic Tricationic surfactants for metallic equipment in oil fields. ACS Omega 5: 26626 – 26639 http://doi.org./10.1021/acsomega.0c03432

[17]. Erazua EA, Adeleke BB (2019) A computational study of quinolone derivatives as corrosion inhibitors for mild steel. J Appl Sci Environ Manage 23: 1819 – 1824 http://doi.org./10.4314/jasem.v23i10.8

[18]. Erteeb MA, Ali-Shattle EE, Khalil SM (2021) Computationl studies (DFT) and PM3 theories on thiophene oligomers as corrosion inhibitors for iron. Americ J Chem 11:1 – 7 http://doi.org./10.5923/j.chemistry.20211101.01

[19]. Fajobi MA, Fayomi OSI, Akande IG (2019) Inhibitive Performance of Ibuprofen Drug on Mild Steel in 0.5 M of H_2SO_4 Acid. J Bio – Tribo Corr 5:1-5. http://doi.org./10.1007/s40735-019-0271-3

[20]. Ugi BU, Obeten M, Bassey VM, BoEkom JB, Omaliko EC, Ugi FB, Uwah IE (2021) Quantum and Electrochemical Studies of Corrosion Inhibition Impact on Industrial Structural Steel (E410) by Expired Amiloride Drug in 0.5 M Solutions of HCl, H_2SO_4 and $NaHCO_3$. *Mor. J. Chem* 9(4): 677-696 https/doi.org/10.48317/IMIST.PRSM/morjchem-v9i3.22346

[21]. Fouda AES, El-Askalany AH, Molouk AFS (2021) Experimental and computational chemical studies on the corrosion inhibitive properties of carbonitrile compounds for carbon steel in aqueous solution. Sci Rep 11: 67 – 79 http://doi.org./10.1038/s41598-021-00701-z

[22]. Geerlings P, Chamorro E, Chattaraj PK (2020) Conceptual density functional theory: status, prospects, issues. Theor Chem Acc. 139: 36 http://doi.org./10.1007/s00214-020-2546-7

[23]. Hsissou R, Abbout S, Seghiri R (2020) Evaluation of corrosion inhibition performance of phosphorus polymer for carbon steel in [1 M] HCl: Computational studies (DFT, MC and MD simulations). J Mater Resear Tech 9: 2691-2703. http://doi.org./10.1016/j.jmrt.2020.01.002

[24]. Jiajun FU, Su-ning L, Wang Y (2020) Computational and electrochemical studies of some amino acid compounds as corrosion inhibitors for mild steel in hydrochloric acid solution, J Mater Sci 45:6255 – 6265 http://doi.org./10.1007/s10853-010-4720-0

[25]. Joshi BD Thakur G Chaudhary MK, (2021) Molecular structure, homo-lumo and vibrational analysis of ergoline by density functional theory. Sci World 14:21–30. http://doi.org./10.3126/sw.v14i14.34978

[26]. Liu Q, Song Z, Han H (2020) A novel green reinforcement corrosion inhibitor extracted from waste Platanus acerifolia leaves. Con Build Mat 260:119695. http://doi.org./10.1016/j.conbuildmat.2020.119695

[27]. Majda MT, Ramezanzadeh M, Ramezanzadeh B (2020) Production of an environmentally stable anti-corrosion film based on Esfand seed extract molecules- metal cations: Integrated experimental and computer modeling approaches. J Hazard Mater 382:1-16. http://doi.org./10.1016/j.hazmat.20192019.121029

[28]. Onyeachu IB, Abdel-Azeim S, Chauhan DS (2021) Electrochemical and Computational insights on the application of expired Metformin drug as a novel inhibitor for the sweet corrosion of C1018 steel. ACS Omega 6 :65 – 76. http://doi.org./10.1021/acsomega.0c03364

[29]. Uwah IE, Ugi BU, Okafor PC (2012) Investigation of the corrosion inhibition effects of Bitters on Mild Steel in acidic medium: A case study of *Andrographis paniculata* and *Vernonia amygdalina,* Proceedings of the 35th Int. Conf. Chem. Soc. Nig 2: 304 – 309

[30]. Padash R, Sajadi GS, Jafari AH (2020) Corrosion control of aluminum in the solutions of NaCl, HCl and NaOH using 2, 6-dimethylpyridine inhibitor: Experimental and DFT insights. Mat Chem Phys 244:122681. http://doi.org./10.1016/j.matchemphys.2020.122681

[31]. Rbaa M, Ouakki M, Galai M (2020) Simple preparation and characterization of novel 8-Hydroxyquinoline derivatives as effective acid corrosion inhibitor for mild steel: Experimental and theoretical studies. Col Surf A: Physicochem Eng Aspects 602:125094. http://doi.org./10.1016/j.colsurfa.2020.125094

[32]. Sharma S, Ganjoo R, Saha SK (2021) Experimental and theoretical analysis of baclofen as a potential corrosion inhibitor for mild steel surface in HCl medium, J Adhs Sci Tech 1: https://doi.org/10.1080/01694243.2021.200230

[33]. Ugi BU, Obeten ME, Bassey VM (2022) Adsorption and inhibition analysis of aconitine and tubocurarine alkaloids as eco-friendly inhibitors of pitting corrosion in ASTM – A47 low carbon steel in hcl acid environment. Indones J Chem 22:1 – 16 http://doi.org./10.22146/ijc.56745

[34]. Solomon MM, Umorena SA, Quraishia MA (2020) Effect of akyl chain length, flow, and temperature on the corrosion inhibition 1 of carbon 2 steel in a simulated acidizing environment by an imidazoline-based inhibitor. J Petrol Sci Eng 2:1-39. http://doi.org./10.1016/j.petrol.2019/106801

[35]. Su P, Li L, Li W (2020) Expired drug theophylline as potential corrosion inhibitor for 7075 aluminum alloy in 1M NaOH solution. Int J Electrochem Sci 15:1412 – 1425. http://doi.org./10.20964/2020.02.25

[36]. Tan J, Guo L, Wu D (2020) Electrochemical and computational studies on the corrosion inhibition of mild steel by 1-Hexadecyl-3-methylimidazolium Bromide in HCl medium. Int. J. Electrochem. Sci 15:1893 – 1903 http://doi.org./10.20964/2020.03.36

[37]. Zaher A, Chaouiki A, Salghi R (2020) Inhibition of mild steel corrosion in 1M hydrochloric medium by the methanolic extract of *Ammi visnaga* l. Lam seeds. Hindawi Int J Corr 1:1 10. http://doi.org./10.1155/2020/9764206

[38]. Xi J, Liu C, Morgan D (2020) An Unexpected Role of H During SiC Corrosion in Water. The J Phys Chem C 124:9394-9400. http://doi.org./10.1021/acs.jpcc.0c02027

[39]. Thanh LT, Vu NSH, Binh PMQ (2020) Combined experimental and computation studies on corrosion inhibition of Houttuynia cordata leaf extract for steel in HCl medium. J Mol Liq 315:113787 http://doi.org./10.1016/j.molliq.2020.113787

Supplementary Files

This is a list of supplementary files associated with this preprint. Click to download.

- GraphicalAbstractChem.Africa.docx